Draft version August 17, 2012
Preprint typeset using LaTeX style emulateapj v. 5/2/11

TRANSIT TIMING VARIATION OF NEAR-RESONANT KOI PAIRS: CONFIRMATION OF 12 MULTIPLE PLANET SYSTEMS

Ji-Wei Xie[1,2]
[1]Department of Astronomy & Key Laboratory of Modern Astronomy and Astrophysics in Ministry of Education, Nanjing University, 210093, China and
[2]Department of Astronomy and Astrophysics, University of Toronto, Toronto, ON M5S 3H4, Canada;
Draft version August 17, 2012

ABSTRACT

We extract Transit Timing Variation (TTV) signals for pairs of transiting planet candidates that are near first-order Mean Motion Resonances (MMR), using publicly available Kepler lightcurves (Q0-Q9). We are able to solidly confirm the planetary nature of 12 new pairs because their TTV signals exhibit sinusoidal variations at the expected timescale and with reasonable phases. Applying the analytical TTV expressions to these systems, we determine planet masses for three pairs of them (KOI 148, 500, 1589), based on the fact that they have nearly zero TTV phase shifts and therefore likely zero free eccentricities. For the remaining nine systems (KOI 152, 248, 829, 869, 877, 880, 898, 1270, and 1336) that show non-zero TTV phase shifts, we are able to obtain their mass upper limits, mass ratios and thus density ratios. Combining another 11 previously confirmed Kepler near-MMR pairs, we find that the whole sample is *generally* consistent with the fiducial mass-radius relation, $m \propto R^{2.06}$, and most of them are like twins with similar sizes and densities, although a few distinct exceptions, such as KOI 148, 869 and Kepler 36. In addition, there seems to be a marginal pattern, i.e., for slightly more pairs, the inner one has a smaller radius but larger density than that of the outer one. Finally, we discuss the uncertainties and implications of our findings.

Subject headings: planetary systems−planets and satellites: detection and dynamical evolution

1. INTRODUCTION

As of today, Kepler mission has found more than 2300 planet candidates (Batalha et al. 2012; Ofir & Dreizler 2012; Huang et al. 2012), and more than 880 of them are multiple transiting candidates (Fabrycky et al. 2012b). One particular interest in these multiple transiting candidates is Transit Timing Variation (TTV), i.e., the deviation of transit time from strict periodicity, which is caused by the gravitational interaction with other planets. By comparing the TTV modelling to the TTV data, one can confirm the existence of planets and/or even constrain their masses and orbits properties (Holman & Murray 2005; Agol et al. 2005). Recently, thanks to this TTV technique, many Kepler planet systems have been confirmed and characterized (Holman et al. 2010; Lissauer et al. 2011b; Cochran et al. 2011; Ford et al. 2012a; Steffen et al. 2012; Fabrycky et al. 2012a; Nesvorný et al. 2012). Most of these planet systems are near Mean Motion Resonance (MMR). This is expected as planets in MMR build up their mutual interactions and thus induce particular large TTV signals.

One of the keys to characterize planets with TTV is to find a good TTV model that can fit the TTV data. To do this, all the above studies rely on N-body simulations to calculate the modelling TTV (Veras et al. 2011). However, due to the considerable number of free parameters, such fits is computationally expensive, and thus it is not practical for characterizing the tons of Kepler candidates. Moreover, the results given by N-body simulations do not have a clear dynamical interpretation of the system. On the other side, recently, Lithwick et al. (2012) (Paper I hereafter) derived a new formulae for the TTV from two near-resonant planets, and proposed a new method to analyze the TTV data. Compared to the method of N-body simulation, the new method is much less time-consuming (hence suitable for analysis of a large sample), and it is straightforward to obtain the mass and eccentricity information of the system.

In this paper, first, we measure and present the TTV of 12 new KOI pairs near first order of MMR, which show strong evidences to confirm their planetary nature. Then, applying the new method (Paper I), we analyze the TTV of each system, which allows us to further extract their masses and orbital eccentricities. This paper is organized as the follows. In §2, we describe our method of TTV measurement and analysis. In §3, we present our results: the overall characteristics of the 12 pairs and their individual properties. In §4, we discuss and summarize the paper.

2. METHOD

2.1. *TTV Measurement*

The data used in this paper are the long cadence (LC), "corrected" light curves (PDC) of KOIs from Q0 to Q9, which are available at Multimission Archive at STScI (MAST[1]).

To measure the mid-transit times of each candidate, we do several irritations as described below.

- *Step 1. Segments.* We first, make a guess of the mid-transiting times using the linear ephemerides based on the epoch and period reported in the catalog of Batalha et al. (2012). Surrounding each mid-transit time, we cut off a segment of light curve

jwxie@astro.utoronto.ca

[1] http://archive.stsci.edu/kepler

with length of 4 times transit duration. Segments which are overlapped by more than one transit duration with segments of other planet candidates are removed. Then, all the selected segments are detrended using a linear based line, and their flux are normalized around unity.

- *Step 2. Template.* Segments from last step are then superimposed and fitted as a whole to form a template using the theoretical transiting model (Mandel & Agol 2002). During the fitting, the epoch, planet-star radius ratio, transit duration, impact parameter, and linear limb-darkening coefficient are allowed to vary.

- *Step 3. Transit Times.* Segments are fitted individually to the template. In each fitting, only the mid-transit time is allowed to vary and all other parameters are fixed on the values given by the last template. The transit time is determined by Levenberg-Marquardt minimization of χ^2, and its uncertainty is estimated from the covariance matrix (Press et al. 1992; Markwardt 2009). The updated transit times are then used as input in step 1 for the next irritation, and they converge generally in two to three irritations.

We tested our TTV measurements by comparing to those already published ones (Holman et al. 2010; Lissauer et al. 2011b; Cochran et al. 2011; Ford et al. 2012a,b; Steffen et al. 2012; Fabrycky et al. 2012a), and found they are generally consistent with each other.

2.2. *TTV Analysis*

In this paper, we focus on planet candidate pairs which are near first order MMR, i.e,

$$\frac{P^{'}}{P} \sim \frac{j}{j-1} \tag{1}$$

where P and $P^{'}$ are the orbital periods of the inner and outer candidates, respectively. Through out this paper, we adopt such a convention: properties of the outer (inner) candidates are denoted with (without) a superscript " $^{'}$ ". The proximity to resonance is defined (see also in Paper I) by

$$\Delta = \frac{P^{'}}{P}\frac{j-1}{j} - 1. \tag{2}$$

Our method of analyzing TTV near resonance has been justified and presented in Paper I. Here, we briefly summarize it and describe the specific procedure used in this paper.

2.2.1. *TTV fitting*

As derived in Paper I, the transit time series of two planets near first order MMR are two linear+sinusoidal curves in the following forms.

$$\begin{aligned} t &= T + P * n + |V|\sin(\lambda^j + \angle V) \\ t^{'} &= T^{'} + P^{'} * n^{'} + |V^{'}|\sin(\lambda^j + \angle V^{'}) \end{aligned} \tag{3}$$

where, t and $t^{'}$, n and $n^{'}$, T and $T^{'}$, P and $P^{'}$ and V and $V^{'}$ are the transit time, transit sequence number, transit offset, transit period, and TTV complex (see Eqn.7) of the inner and outer planets, respectively. And

$$\begin{aligned} \lambda^j &= j\lambda^{'} - (j-1)\lambda \\ &= -\frac{2\pi}{P^{'}/j\Delta}(t - T^{'}) + \frac{2\pi}{P}(j-1)(T - T^{'}) \end{aligned} \tag{4}$$

is the *longitude of conjunctions*, where $\lambda = \frac{2\pi}{P}(t-T)$ and $\lambda^{'} = \frac{2\pi}{P^{'}}(t-T^{'})$ are the mean longitudes of the inner and outer planet, respectively. The TTV period, which we call *super-period*, is

$$P^j = \frac{P^{'}}{j|\Delta|}, \tag{5}$$

and

$$\begin{aligned} A_{ttv} = |V|, \qquad A^{'}_{ttv} = |V^{'}| \\ \phi_{ttv} = \angle\left(\frac{\Delta}{|\Delta|}V\right),\ \phi^{'}_{ttv} = \angle\left(\frac{\Delta}{|\Delta|}V^{'}\right) \end{aligned} \tag{6}$$

are the TTV amplitude and phase, respectively.

To fit the TTV measurements we perform the following procedure.

- *Step 1.* Fit the transit times with linear formula, which give us the first guesses of $T(T^{'})$ and $P(P^{'})$.

- *Step 2.* Calculate λ^j using the $T(T^{'})$ and $P(P^{'})$ obtained from last fitting.

- *Step 3.* Refit the transit times using Eqn.3 to get new $T(T^{'})$, $P(P^{'})$ and $V(V^j)$. Note, in this fitting, all λ^j are fixed on the values obtained at step 2. The best fit is determined by Levenberg-Marquardt minimization of χ^2, and the uncertainties of fit parameters are estimated from the covariance matrix (Press et al. 1992; Markwardt 2009).

- *Step 4.* Calculate the relative differences between $T(T^{'})$, $P(P^{'})$, P^j and those obtained from last fit. If all these differences are less than 10^{-3}, then choose the latest fit as the final result, otherwise goto step 2. Generally, the fitting converge in less than five loops.

The direct goal of the above TTV fitting is to obtain the TTV amplitude and phase, as well as their error bars and the goodness of the fit.

2.2.2. *TTV interpretation*

The advantage of this TTV analyzing method is that the TTV amplitude and phase (or TTV complex) explicitly reveal the masses and eccentricity of the system (Paper I), i.e.,

$$\begin{aligned} V &= P\frac{\mu^{'}}{\pi j^{2/3}(j-1)^{1/3}\Delta}\left(-f - \frac{3}{2}\frac{Z^*_{\rm free}}{\Delta}\right) \\ V^{'} &= P^{'}\frac{\mu}{\pi j\Delta}\left(-g + \frac{3}{2}\frac{Z^*_{\rm free}}{\Delta}\right), \end{aligned} \tag{7}$$

where μ and $\mu^{'}$ are the mass ratio of the inner and outer planets to the star, respectively, f and g are sums of

Laplace coefficients, as listed in Table A1 of Paper I, and $Z^*_{\rm free}$ is the complex conjugate of $Z_{\rm free} = fz_{\rm free} + gz^{'}_{\rm free}$, a linear combination of the free complex eccentricities of the two planets. For typical Kepler system considered here, $\mu \leq 10^{-4}$, $\mu^{'} \leq 10^{-4}$, and $|\Delta| \geq 10^{-2}$, then the forced eccentricities of the two planets are relative small, i.e., $|z_{forced}| \sim \mu/|\Delta| \leq 10^{-2}$ and $|z^{'}_{forced}| \sim \mu^{'}/|\Delta| \leq 10^{-2}$. Thus, taking an approximation of order of unity, $|Z^*_{\rm free}|$ in Eq.7 could be considered as the true eccentricity of the two planets.

In principle, μ, $\mu^{'}$ and $Z^*_{\rm free}$ (both real and imaginary parts) can be inferred by inverting Eqn. 7. In reality, however, $Z^*_{\rm free}$ is highly degenerated with μ and/or $\mu^{'}$ (Paper I). Nevertheless, as argued in Paper I, one can use the TTV phases distribution (Eqn.6) to statistically estimate the masses and eccentricity. If the phases are close to $\phi_{ttv} = 0$ and $\phi^{'}_{ttv} = 180^\circ$ then the system probably have very small free eccentricity, and the masses of the two planets are likely to be the nominal masses solved from Eqn.7 by assuming $|Z^*_{free}| = 0$, i.e.,

$$m_{nom} = M_\star \left| \frac{V^{'}\Delta}{P^{'}g} \right| \pi j$$
$$m^{'}_{nom} = M_\star \left| \frac{V\Delta}{Pf} \right| \pi j^{2/3}(j-1)^{1/3}, \quad (8)$$

Otherwise, if the phase are significantly away from $\phi_{ttv} = 0$ and $\phi^{'}_{ttv} = 180^\circ$, then it indicates large eccentricities of the system, and the nominal masses are likely their upper limits.

Furthermore, we can estimate the mass ratio of the pair from Eqn.7, i.e.,

$$\frac{m^{'}}{m} \sim \left(\frac{|V|^{'}}{|V|}\right)^{-1} \left(\frac{P^{'}}{P}\right) \left(\frac{g}{f}\right) \left(\frac{j-1}{j}\right) \quad \text{if } Z_{\rm free} \ll |\Delta|$$
$$\frac{m^{'}}{m} \sim \left(\frac{|V|^{'}}{|V|}\right)^{-1} \left(\frac{P^{'}}{P}\right) \left(\frac{j-1}{j}\right) \quad \text{if otherwise.} \quad (9)$$

which allows us to further obtain their density ratio $\rho^{'}/\rho$. Note the two mass ratios in Eqn.9 are comparable to each other except for the case of 2:1 MMR, where they differ by a factor of ~ 3.

3. RESULTS

3.1. *Overview*

We plot the TTV data for the 12 systems in Fig.1-4. Their TTV generally follow the theoretical curves with expected period and reasonable phases, suggesting that they are real planets pairs near MMR. Further TTV analyses reveal the masses and orbital eccentricities of each system. Table 1 and table 2, respectively, summarize the key physical properties and the results of TTV analyses of the 12 planetary systems confirmed in this paper. To visualize the whole results, we plot all the systems in the TTV phase diagram (Fig.5), mass-radius diagram (Fig.6), and radius-density diagram (Fig.7).

3.1.1. *TTV phase diagram*

We plot in Fig.5 the TTV phase of inner one vs. that of the outer one for each pair. One striking feature is that almost no system is located in quadrants II and IV[2], i.e., theoretically forbidden region. This is another independent evidence showing that these candidates are real interacting planets near MMR, otherwise the phase distribution should not follow the theoretical prediction but probably be random. Furthermore, the location of each system in the TTV phase diagram reveals the dynamical information of the system. As justified in Paper I, generally, systems with little phase shift, i.e., close to $(0, \pi)$, including KOI 148, 500 and 1589, are likely to have zero free eccentricities and their masses are likely close to the nominal masses. While other systems with significant phase shift, including KOI 152, 248, 829, 869, 877, 880, 898, 1270 and 1336, are likely have significant free eccentricities (on the order of Δ or even larger), and the nominal masses are likely their upper limits.

3.1.2. *mass-radius diagram*

We plot the nominal mass vs. radius size for each planet (24 in total) in Fig.6. As can be seen in this mass-radius diagram, most of them have radii between 2-4 $R_\oplus$ and density around that of the Neptune and the Earth. Some systems are located at extremely high density region, including 152.01, 829.01, 869.03, 1270.01. For these systems, such high densities should be considered only as upper limits. In fact, the true densities could be much smaller given that (1) the true masses are much lower than the nominal mass because of significant free eccentricities in these system, or (2) the planetary radii might be underestimated given their relative large uncertainties (see §4.1). If the radius increases by 25% then the planet density will drop by a factor of 2. In addition, KOI 152, 500, and 1589 are systems potentially involved in resonance chains. Further individual analyses (§3.2) show that KOI 152.03 and 152.02 are likely affected by the resonance chain and the masses shown here might not fully reflect their true masses, and the resonance chain effect is less important to KOI 1589.01 and 1589.02 but unclear to KOI 500.01 and 500.02.

3.1.3. *radius-density diagram*

We calculate the density ratio, i.e., $\rho^{'}/\rho$ (outer over inner) for all the 12 pairs plus 11 pairs of previous confirmed Kepler planets, and plot them vs. $R^{'}/R$ in Fig.7. Ons striking feature is that all the system as a whole show a trend: density decreases with radius, which is constant with the theory of planetary internal structure and generally follows the fiducial mass-radius relation, i.e., $m \propto R^{2.06}$ (Lissauer et al. 2011a). Furthermore, for most systems, they are close to the origin, suggesting the two planets of each pair are like twins with similar sizes and densities. Nevertheless, there are some systems, such as KOI 869, 1270 and Kepler 36 , with two planets near MMR having very different sizes and densities. In addition, there seems to be a pattern, although marginally, i.e., for slightly more pairs, the inner member has a smaller radius but larger density than that of the

[2] Given the relative large phase uncertainty, it is reasonable that some of them, such as KOI 148, 877 and 880, are near the boundary which separate the allowed and forbidden zones.

outer one. Finally, we caution that the results shown in this figure subject to large uncertainties, especially for KOI 869, 877, 898 and 1270.

3.2. *Individual Systems*

1. *KOI 148.01 and 148.02*
The KOI 148 system has three transiting objects 148.01, 148.02 and 148.03, with orbital periods about 4.78, 9.67 and 42.90 d and radii about 2.1, 3.1 and 2.4 $R_\oplus$, respectively. The inner two are near 2:1 MMR with $\Delta = 0.012$ and show expected TTV (Fig.1). Their TTV phases are near the boundary between allowed and forbidden zones but close to $(0, \pi)$, suggesting that they are likely to have zero free eccentricities and their masses are close to the nominal mass, $m \sim 14.3$ and $m^{'} \sim 9.2$ $M_\oplus$. The outer objects, 148.03, is not close to any MMR and thus should have little contamination to the TTV of the inner pair.

2. *KOI 152.03 and 152.02*
The KOI 152 system has three transiting objects 152.03, 152.02 and 152.01, with orbital periods about 13.5, 27.4 and 52.1 d and radii about 2.6, 2.8 and 5.8 $R_\oplus$, respectively. The inner two have a orbital ratio of 2.037 and thus near 2:1 MMR with $\Delta = 0.018$ and an expected TTV period of 851 day, which is clearly shown from both their TTV periodograms. Their TTV phases have significant shift away from $(0, \pi)$, suggesting they are likely to have significant free eccentricities (on the order of Δ at least). Combining their TTV amplitudes, we estimate their mass ratio to be $m^{'}/m \sim 0.48$, density ratio $\rho^{'}/\rho \sim 0.40$, and their mass upper limits $m_{nom} = 65.3$ and $m^{'}_{nom} = 10.1$ $M_\oplus$.
Note, above results ignored the effect of object 152.01, which has a period ratio about 1.9 and thus $\Delta = 0.05$ with 152.02. Although such an outer pair is much further away from 2:1 MMR as compared to the inner pair, it could still has a significant impact given the relative large radius of 152.01. As can be seen from Fig.1), the TTV periodogram of 152.02 has a broad power distribution from period 500-1000 d, which is consistent with both super-periods of the inner ($P^j = 851$ d) and outer ($P^j = 526$ d) pairs, and thus leads to comparable fits for the TTV data 152.02 in both cases. In addition, the TTV periodogram of 152.01 also show some weak peaks around $P^j = 526$ d. All of these clues lead us to conclude that the TTV of the inner pair, i.e., 152.03 and 152.02, is contaminated by 152.01, and the results of our TTV analysis given in table 1 and 2 might not fully reflect the nature of this system. This system is particularly interesting for future studies on modelling the TTV of a resonant chain, which may provide further valuable insight into the dynamics of 3-body resonance.

3. *KOI 248.01 and 248.02*
The KOI 248 system has four transiting objects 248.03, 248.01, 248.02 and 248.04 with orbital periods about 2.58, 7.20, 10.91 and 18.60 d and radii about 1.9, 2.7, 2.5 and 2.0 $R_\oplus$, respectively. The middle two, 248.01 and 248.02 are near 3:2 MMR with $\Delta = 0.01$ and show expected TTV (Fig.1). Their TTV phases (Fig.5) have significant shift away from $(0, \pi)$, suggesting they are likely to have significant free eccentricities (on the order of Δ at least). Combining their TTV amplitudes, we estimate their mass ratio to be $m^{'}/m \sim 0.60$, density ratio $\rho^{'}/\rho \sim 0.73$, and their mass upper limits $m_{nom} = 8.9$ and $m^{'}_{nom} = 6.7$ $M_\oplus$. The other two smaller objects 248.03 and 248.04 are not involved in any first or second order of MMR and thus should have little contamination to the TTV of the middle pair.

4. *KOI 500.01 and 500.02*
The KOI 500 system has five transiting objects 500.05, 500.03. 500.04, 500.01 and 500.02 with orbital periods about 0.99, 3.07, 4.65, 7.05 and 9.52 d and radii about 1.4, 1.5, 1.6, 2.6 and 2.8 $R_\oplus$, respectively. The outer two, 500.01 and 500.02 are near 4:3 MMR with $\Delta = 0.012$ and show expected TTV (Fig.1). Their TTV phases are close to $(0, \pi)$, suggesting that they are likely to have zero free eccentricities and their masses are close to the nominal mass, $m \sim 6.2$ and $m^{'} \sim 10.5$ $M_\oplus$.
For the inner three smaller objects, 500.05 is not involved in any MMR, and 500.03 and 500.04 are close to 3:2 MMR. In addition, 500.04 and 500.01 are close to 3:2 MMR, and 500.04 and 500.02 are close to 2:1 MMR. In total, there are 4 pairs near MMR in the system of KOI 500, and interestingly, all of them have nearly identical super-period, P^j ∼191-192 d. Nevertheless, as seen in Fig.2, only 500.01 and 500.02 show the expected TTV, and the other objects seem to have little effects (probably because their relative smaller sizes and thus likely smaller masses). In any case, KOI 500 is a particularly interesting system with 4 bodies involved in 4 MMR of the same super-period. Future studies are needed to further unveil such a peculiar system.

5. *KOI 829.01 and 829.02*
The KOI 829 system has three transiting objects 829.02, 829.01 and 829.03 with orbital periods about 9.75, 18.65 and 38.56 d and radii about 1.9, 2.9 and 3.2 $R_\oplus$, respectively. The outer two, 829.01 and 829.03 are near 2:1 MMR with $\Delta = 0.034$ and show expected TTV (Fig.3). Their TTV phases (Fig.5) have significant shift away from $(0, \pi)$, suggesting they are likely to have significant free eccentricities (on the order of Δ at least). Combining their TTV amplitudes, we estimate their mass ratio to be $m^{'}/m \sim 1.23$, density ratio $\rho^{'}/\rho \sim 0.93$, and their mass upper limits $m_{nom} = 91.1$ and $m^{'}_{nom} = 30.5$ $M_\oplus$. Note, in 2:1 MMR, the true mass of the inner one may differ a lot from its nominal mass even if the free eccentricity is small. For example, if $|Z_{free}| = \Delta = 0.034$, then the true mass of 829.01 is likely smaller than its nominal mass by a factor of 4 (Eqn.7), i.e., $m \sim 23$ $M_\oplus$. The inner smaller object, 829.02, is not close to any MMR and thus should have little contamination to the

TTV of the middle pair.

6. *KOI 869.03 and 869.02*
The KOI 869 system has four transiting objects 869.04, 869.01, 869.03 and 869.02 with orbital periods about 3.22, 7.49, 17.46 and 36.28 d and radii about 1.8, 2.7, 2.7 and 3.2 $R_\oplus$, respectively. The outer two, 869.03 and 869.02 are near 2:1 MMR with $\Delta = 0.039$ and show expected TTV (Fig.3). Their TTV phases (Fig.5) have significant shift away from $(0, \pi)$, suggesting they are likely to have significant free eccentricities (on the order of Δ at least). Combining their TTV amplitudes, we estimate their mass ratio to be $m^{'}/m \sim 0.28$, density ratio $\rho^{'}/\rho \sim 0.16$, and their mass upper limits $m_{nom} = 295.0$ and $m^{'}_{nom} = 21.4$ $M_\oplus$.

Note, in 2:1 MMR, the true mass of the inner one may differ a lot from its nominal mass even if the free eccentricity is small. For example, if $|Z_{free}| = \Delta = 0.039$, then the true mass of 869.03 is likely smaller than its nominal mass by a factor of 4 (Eqn.7), i.e., $m \sim 75$ $M_\oplus$. Such a mass may still be too high and thus cause an unrealistically high density of ~ 21 g cm^{-3} for 869.03. Two possibilities or their combination may solve this density problem. One could be that the free eccentricity of the system is larger. If $|Z_{free}| > 0.1$ then the density of 869.03 will drop below ~ 8 g cm^{-3}. The other possibility could be the radii of the planet are underestimated (see discussion in §4.1). If the radius increase by 25%, then the density of 869.03 will drop by a factor of 2. In any case, the density ratio $\rho^{'}/\rho \sim 0.16$ should be maintained (caution large uncertainties shown in table 1). Such a large contrast in density is also observed recently in Kepler 36b and 36c.

The inner two objects, 869.04 and 869.01, are not close to any MMR and thus has little contamination to the TTV of the outer pair.

7. *KOI 877.01 and 877.02*
The KOI 877 system has only two transiting objects 877.01 and 877.02 with orbital periods about 5.95 and 12.04 d and radii about 2.4 and 2.4 $R_\oplus$, respectively. The two planets are near 2:1 MMR with $\Delta = 0.011$ and show expected TTV (Fig.3). Their TTV phases (Fig.5) have significant shift away from $(0, \pi)$, suggesting they are likely to have significant free eccentricities (on the order of Δ). Combining their TTV amplitudes, we estimate their mass ratio to be $m^{'}/m \sim 0.57$, density ratio $\rho^{'}/\rho \sim 0.60$ (caution large uncertainties shown in table 1), and their mass upper limits $m_{nom} = 21.4$ and $m^{'}_{nom} = 4.0$ $M_\oplus$.

8. *KOI 880.01 and 880.02*
The KOI 880 system has four transiting objects 880.04, 880.03, 880.01 and 880.02 with orbital periods about 2.38, 5.90, 26.44 and 51.53 d and radii about 1.4, 2.3, 4.0 and 5.3 $R_\oplus$, respectively. The larger outer two, 880.01 and 880.02 are near 2:1 MMR with $\Delta = -0.026$ and show expected TTV (Fig.4). Their TTV phases (Fig.5) have significant shift away from $(0, \pi)$, suggesting they are likely to have significant free eccentricities (on the order of Δ). Combining their TTV amplitudes, we estimate their mass ratio to be $m^{'}/m \sim 0.82$, density ratio $\rho^{'}/\rho \sim 0.34$, and their mass upper limits $m_{nom} = 50.9$ and $m^{'}_{nom} = 17.4$ $M_\oplus$. The other two smaller objects 880.04 and 880.03 are not involved in any first or second order of MMR and thus should have little contamination to the TTV of the middle pair.

9. *KOI 898.01 and 898.03*
The KOI 898 system has three transiting objects 898.02, 898.01 and 898.03 with orbital periods about 5.17, 9.77 and 20.09 d and radii about 2.2, 2.8 and 2.4 $R_\oplus$, respectively. The outer two, 898.01 and 898.03 are near 2:1 MMR with $\Delta = 0.028$ and show expected TTV (Fig.4). Their TTV phases (Fig.5) have significant shift away from $(0, \pi)$, suggesting they are likely to have significant free eccentricities (on the order of Δ at least). Combining their TTV amplitudes, we estimate their mass ratio to be $m^{'}/m \sim 1.11$, density ratio $\rho^{'}/\rho \sim 1.92$ (caution large uncertainties shown in table 1), and their mass upper limits $m_{nom} = 44.7$ and $m^{'}_{nom} = 14.3$ $M_\oplus$. Note, in 2:1 MMR, the true mass of the inner one may differ a lot from its nominal mass even if the free eccentricity is small. For example, if $|Z_{free}| = \Delta = 0.028$, then the true mass of 898.01 is likely smaller than its nominal mass by a factor of 4 (Eqn.7), i.e., $m \sim 11$ $M_\oplus$. The other inner objects 898.02 is not close to any first or second order of MMR and thus should have little contamination to the TTV of the outer pair.

10. *KOI 1270.01 and 1270.02*
The KOI 1270 system has only two transiting objects 1270.01 and 1270.02 with orbital periods about 5.73 and 11.61 d and radii about 2.2 and 1.6 $R_\oplus$, respectively. The two planets are near 2:1 MMR with $\Delta = 0.013$ and show expected TTV (Fig.4). Their TTV phases (Fig.5) have significant shift away from $(0, \pi)$, suggesting they are likely to have significant free eccentricities (on the order of Δ at least). Combining their TTV amplitudes, we estimate their mass ratio to be $m^{'}/m \sim 0.14$, density ratio $\rho^{'}/\rho \sim 0.39$(caution large uncertainties shown in table 1), and their mass upper limits $m_{nom} = 132.8$ and $m^{'}_{nom} = 6.0$ $M_\oplus$. Note, in 2:1 MMR, the true mass of the inner one may differ a lot from its nominal mass even if the free eccentricity is small. For example, if $|Z_{free}| = \Delta = 0.013$, then the true mass of 1270.01 is likely smaller than its nominal mass by a factor of 4 (Eqn.7), i.e., $m \sim 33$ $M_\oplus$. Such a mass may still be too high and thus cause an unrealistically high density of ~ 17 g cm^{-3} for 1270.01. Two possibilities or their combination may solve this density problem. One could be that the free eccentricity of the system is larger. If $|Z_{free}| > 0.03$ then the density of 1270.01 will drop below ~ 8 g cm^{-3}. The other possibility

could be the radii of the planet are underestimated (see discussion in §4.1). If the radius increase by 25%, then the density of 1270.01 will drop by a factor of 2. Indeed, we note there are quite large uncertainties on the planet radii of system KOI 1270 (see table 1.

11. *KOI 1336.01 and 1336.02*
The KOI 1336 system has only two transiting objects 1336.01 and 1336.02 with orbital periods about 10.22 and 15.57 d and radii about 2.8 and 2.9 $R_\oplus$, respectively. The two planets are near 3:2 MMR with $\Delta = 0.016$ and show expected TTV (Fig.4). Their TTV phases (Fig.5) have significant shift away from $(0, \pi)$, suggesting they are likely to have significant free eccentricities (on the order of Δ at least). Combining their TTV amplitudes, we estimate their mass ratio to be $m^{'}/m \sim 0.89$, density ratio $\rho^{'}/\rho \sim 0.82$, and their mass upper limits $m_{nom} = 23.9$ and $m^{'}_{nom} = 26.4$ $M_\oplus$.

12. *KOI 1589.01 and 1589.02*
The KOI 1589 system has five transiting objects 1589.04, 1589.01, 1589.02, 1589.03 and 1589.05 with orbital periods about 4.22, 8.73, 12.88, 27.43 and 44.55 d and radii about 1.3, 2.2, 2.4, 2.4, and 2.0 $R_\oplus$, respectively. 1589.01 and 1589.02 are near 3:2 MMR with $\Delta = -0.016$ and show expected TTV (Fig.4). Their TTV phases are close to $(0, \pi)$, suggesting that they are likely to have zero free eccentricities and their masses are close to the nominal mass, $m \sim 17.6$ and $m^{'} \sim 16.5$ $M_\oplus$.

For the other three objects, the outer two, 1589.03 and 1589.05, are not close to any first or second order of MMR and should have little contamination to the TTV of 1589.01 and 1589.02. The innermost one, 1589.04, is close to 2:1 MMR with 1589.01. Such a pair have a $\Delta = 0.033$ and super-period of $P^j = 133$ d. Considering the relative large Δ (proximity to resonance, which is two times larger than that of the pair 1589.01 and 1589.02), and the relative smaller radius of 1589.04 as compared to 1589.01, we expect that 1589.04 should have little contamination to the TTV of 1589.01 and 1589.02. Indeed, there is no evident signal in the TTV of 1589.01 with period close to the super-period ($P^j = 133$ d) of the pair 1589.04 and 1589.01.

4. SUMMARY AND DISCUSSION

A large number of transiting exoplanet candidates have been, and would continually be found by the Kepler mission, raising the demand for an efficient method to confirm and characterize the planetary nature of these candidates. Measuring and analyzing TTV is a promising technique to fill the above need, and it has been demonstrated to be highly successful, especially for those multiple transiting candidates near MMR(Holman et al. 2010; Lissauer et al. 2011b; Cochran et al. 2011; Ford et al. 2012a; Fabrycky et al. 2012a; Steffen et al. 2012). However, all these studies, rely on fitting the TTV data to direct N-body simulations, which is computationaly time-consuming and thus more suitable to detail analysis of individual systems.

In this paper, we extract TTV signals for 12 systems of transiting planet candidates that are near first-order MMR, using publicly available Kepler lightcurves through Q9. Their TTV (Fig.1-4) generally follow the theoretical curves with expected period and reasonable phases, suggesting that they are real planets pairs near MMR. Based on the new analytical formulae for the TTV from two near-resonant planets (Paper I), we are able to develop an efficient method for analyzing the whole sample of TTV data. The direct results (table 2) of this TTV analysis progress are the TTV amplitude and phase (or called TTV complex together, defined in the TTV formulae at §2.3 and/or Paper I), which reveal the information of the mass and eccentricity of the system (see Fig.5-7 and table 1). We summarize our major findings in the following.

- Three systems KOI 148, 500 and 1589 are likely to have zero free eccentricities and their masses are likely close to the nominal mass (Eq.8). For the other nine systems with significant free eccentricities (on the order of Δ at least), we derive their mass upper limits, mass ratios and density ratio (caution the large error bars).

- Three systems, KOI 152, 500, and 1589, are close to resonance chains. We find that pair KOI 152.03-02 are likely affected by the resonance chain induced by 152.01, therefore the results of their TTV analysis shown here might probably be contaminated. The resonance chain effect is found to be unlikely to affect the TTV analyses of KOI 1589.01-02 and KOI 500.01-02.

- Combining another 11 previously confirmed near-MMR KOI pairs, we find (1) the whole sample is *generally* consistent with the fiducial mass-radius relation $m \propto R^{2.06}$ (Lissauer et al. 2011a), (2) most pairs are like twins with similar sizes and densities (caution the large error bars, see §4.1), although some pairs with dramatic differences in sizes and densities of their members, and (3) a marginal pattern, i.e., for slightly more pairs, the inner member has a smaller radius but larger density than that of the outer one. All these clues provide valuable insights into the origin of such near-MMR parirs (see §4.2).

4.1. *Uncertainties of Stellar and Planetary Radii*

Planetary radius is determined by the product of two independent quantities: planet-star radius ratio, which is based on the modelling transit light curves, and stellar radius, which is based on our knowledge of the host star. The radii of the planets confirmed in this paper are adopted from the catalog of Batalha et al. (2012), and their uncertainties plotted in Fig.6 and table 1 only reflect the uncertainties on individual fits of transit light curves. We caution the true uncertainties are likely underestimated given the consideration of the following aspects.

- *Systematic uncertainty of planet-star radius ratio* could be induced by the different methods and models used to analyze the transit light curves, such as the specific way for detrending and folding

the light curves and the specific limb darkening law used in fitting the transit light curves. For a simple diagnosis, we compared planet-star radius ratio measurements of 60 Kepler confirmed planets from the KOI catalog (Batalha et al. 2012) and those reported in papers which individually claimed the confirmation of such planets. As can be seen in the middle panel of Fig.8, the standard deviation of such two kinds of measurements is 12.6%, which may reflect the order of magnitude of the systematic uncertainty of planet-star radius ratio.

- *Uncertainties of stellar radii* are not given in the KOI catalog (Batalha et al. 2012), but can be generally estimated by comparing the stellar radii given but different studies. We perform such an analysis to 37 KOIs in the top panel of Fig.8. As can be seen, the stellar radii from (Batalha et al. 2012) tend to be systematically underestimated by $\sim 7\%$ and has a standard deviation of $\sim 28\%$ as compared to those given by individual confirming papers.

In the bottom panel of Fig.8, we plot the deduced planetary radii of 60 Kepler confirmed planets from individual confirming papers vs. those from the KOI catalog (Batalha et al. 2012). According to principle of error propagation, we expect that the uncertainty of the planetary radii should be the sum of both uncertainties of planet-star radius ratio and stellar radius. As can be seen, the planetary radius deviation of 29%, although lower than the above expectation by $\sim 12\%$ [3], could still cause a large deviation in planet density of a factor of ~ 2. Future high-precision spectroscopic follow-up observations which can help accurately determine stellar radius are required to better characterize these KOI systems.

4.2. *Origin of the near-MMR pairs*

One striking feature of the near-MMR KOI pairs is the asymmetric distribution around the nominal resonance center, i.e., most of them have a period ratio which is a few percents larger than the exact commensurability.(Fabrycky et al. 2012b). Such a feature is also seen in the 12 planets confirmed in this paper, among which 2 of them with negative Δ while the other 10 with positive Δ. Recently, it has been suggested that such an asymmetry might be induced by some dissipation processes, e.g., tides, which damp the eccentricities of planets in MMR and lead to a slow divergence away from exact commensurability (Terquem & Papaloizou 2007; Batalha et al. 2012; Lithwick & Wu 2012). One prediction of such an dissipation scenario is that the near-MMR pairs should have zero-free eccentricities because of eccentricity damping. Although this seems to be confirmed by some systems (KOI 148, 500 and 1529), we caution that all the other systems have small but significantly finite free eccentricities on a order of a few percents (similar results were also abstained in Paper I). This may imply either planets could reacquire free eccentricities after dissipation via some certain processes or maybe the asymmetric feature was caused by some other unknown mechanisms.

More clues might be revealed from the radius-density diagram (Fig.7). As can be seen, most paris are clustered near the origin where $\rho^{'} = \rho$ and $R^{'} = R$, which might indicate that most of them are randomly paired together with similar sizes and densities. Such a result is consistent with that of Fabrycky et al. (2012b), which finds that all paris in all KOI systems are likely drawn from a smooth distribution of period ratios, and they do not necessarily point to differential migration. Although these clues seems to support an insitu scenario (Hansen & Murray 2012) for the formation of those pairs, we caution that an non-insitu scenario associated with migration, if not dominant, might still be suitable for explaining the marginal radius-density pattern, namely more pairs with the inner member smaller but denser than the outer one, such as Kepler 36 and KOI 869. The general explanation from the migration scenario could be that the currently near-resonant pair were not formed near each other, but widely separated in the protoplanetary disk. As the disk is cooler and hill radius is larger (thus larger feeding zone when the planet was formed) outside, the outer planet accreted more volatile material and finally became larger but less dense than the inner one. After their formation, interactions with the disk could then enable them to migrate to the present location (Lee & Peale 2002; Zhou et al. 2005; Terquem & Papaloizou 2007).

The current results shown in this paper are subject to relatively large uncertainties both on planet mass and radius. Further TTV data and high-precision spectroscopic follow-up observations of the host stars in the future will reduce such error bars, thus allow a better characterization to each system and provide a clearer picture on the origin of the near-MMR pairs.

JWX acknowledges support from the Ontario government, the National Natural Science Foundation of China (Nos. 10833001 and 10925313), Fundamental Research Funds for the Central Universities (No.1112020102), Research Fund for the Doctoral Program of Higher Education of China (No.20090091110002), and Nanjing University. JWX thanks the whole Kepler team for producing such beautiful light curves.

REFERENCES

Agol, E., Steffen, J., Sari, R., & Clarkson, W. 2005, MNRAS, 359, 567
Baraffe, I., Selsis, F., Chabrier, G., et al. 2004, A&A, 419, L13
Batalha, N. M., Borucki, W. J., Bryson, S. T., et al. 2011, ApJ, 729, 27
Batalha, N. M., Rowe, J. F., Bryson, S. T., et al. 2012, arXiv:1202.5852
Batygin, K., & Morbidelli, A. 2012, arXiv:1204.2791
Cochran, W. D., Fabrycky, D. C., Torres, G., et al. 2011, ApJS, 197, 7
Fabrycky, D. C., Ford, E. B., Steffen, J. H., et al. 2012, ApJ, 750, 114
Fabrycky, D. C., Lissauer, J. J., Ragozzine, D., et al. 2012, arXiv:1202.6328

[3] This might be caused by that either planet-star ratio and stellar radius are not fully independent of each other or the samples (37 stars and 60 planets) studied here are not large enough

Ford, E. B., Fabrycky, D. C., Steffen, J. H., et al. 2012, ApJ, 750, 113
Ford, E. B., Ragozzine, D., Rowe, J. F., et al. 2012, arXiv:1201.1892
Fressin, F., Torres, G., Désert, J.-M., et al. 2011, ApJS, 197, 5
Hansen, B. M. S., & Murray, N. 2012, ApJ, 751, 158
Holman, M. J., & Murray, N. W. 2005, Science, 307, 1288
Holman, M. J., Fabrycky, D. C., Ragozzine, D., et al. 2010, Science, 330, 51
Huang, X., Bakos, G. Á., & Hartman, J. D. 2012, arXiv:1205.6492
Lee, M. H., & Peale, S. J. 2002, ApJ, 567, 596
Lissauer, J. J., Fabrycky, D. C., Ford, E. B., et al. 2011, Nature, 470, 53
Lissauer, J. J., Ragozzine, D., Fabrycky, D. C., et al. 2011, ApJS, 197, 8
Lithwick, Y., & Wu, Y. 2012, ApJ, 756, L11
Lithwick, Y., Xie, J., & Wu, Y. 2012, arXiv:1207.4192
Mandel, K., & Agol, E. 2002, ApJ, 580, L171
Markwardt, C. B. 2009, Astronomical Data Analysis Software and Systems XVIII, 411, 251
Nesvorný, D., Kipping, D. M., Buchhave, L. A., et al. 2012, Science, 336, 1133
Ofir, A., & Dreizler, S. 2012, arXiv:1206.5347
Press, W. H., Teukolsky, S. A., Vetterling, W. T., & Flannery, B. P. 1992, Cambridge: University Press, c1992, 2nd ed.,
Steffen, J. H., Fabrycky, D. C., Ford, E. B., et al. 2012, MNRAS, 421, 2342
Terquem, C., & Papaloizou, J. C. B. 2007, ApJ, 654, 1110
Veras, D., Ford, E. B., & Payne, M. J. 2011, ApJ, 727, 74
Zhou, J.-L., Aarseth, S. J., Lin, D. N. C., & Nagasawa, M. 2005, ApJ, 631, L85

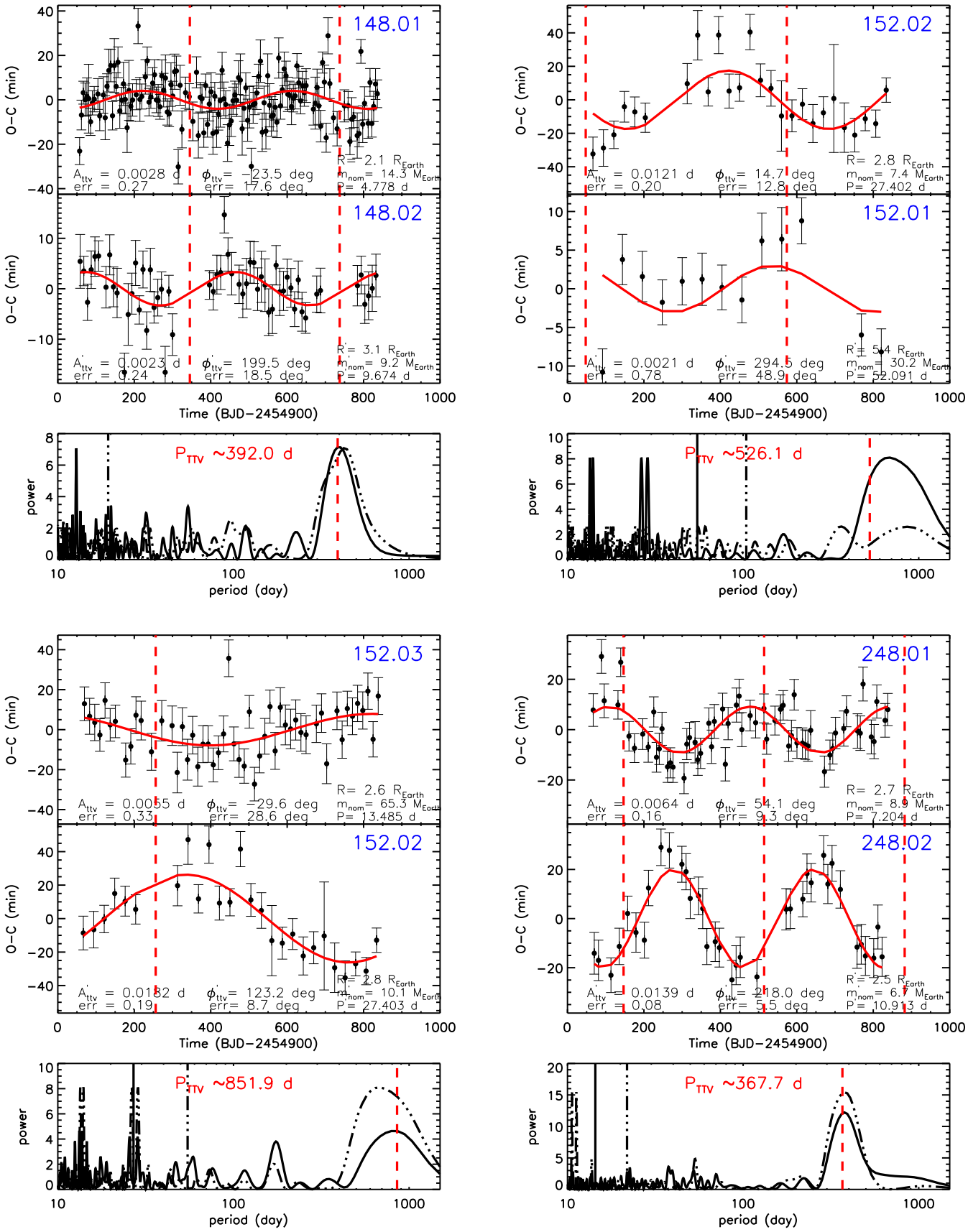

FIG. 1.— TTV evidences of four candidate paris. For each of them, we plot the best-fit theoretical curves on top of the TTV data and the TTV periodogram. In the TTV fitting panels, The vertical dashed lines denote the times when the longitude of conjunction points at the observer, i.e., $\lambda^J = 0$. In the periodogram panel, the red vertical dashed line denotes the theorectically predicted period of the TTV, and the two other vertical lines denotes the periods corresponding to the Nyquist critical frequencies of the two planets, respectively. The TTV fitting results: amplitude (A_{ttv}) and its normalized error, phase (ϕ_{ttv}) and its absolute error, planet radius (R), nominal mass (m_{nom}), and orbital period (P) are also shown in each TTV fitting panel.

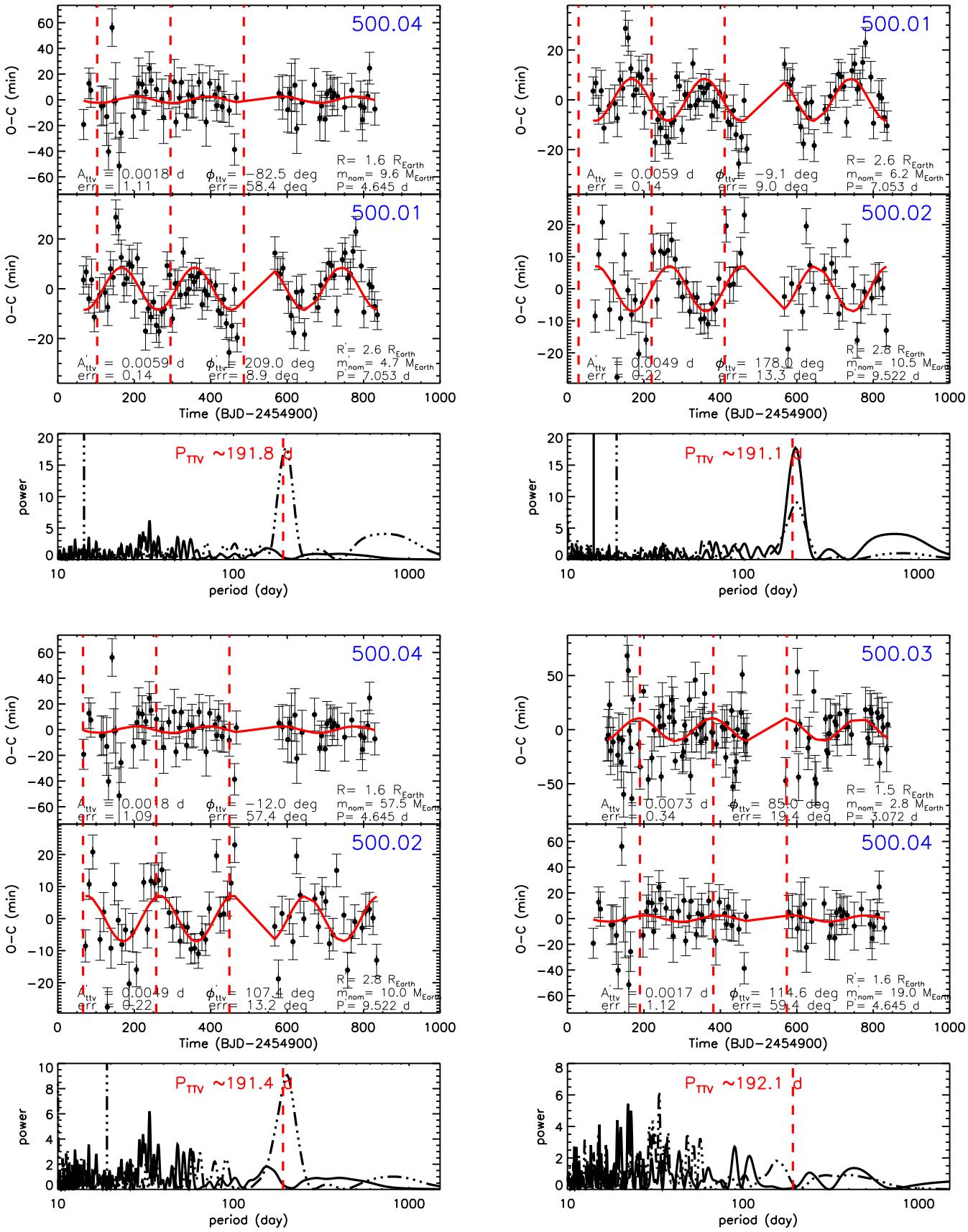

FIG. 2.— Similar to Fig.1, but for another four pairs.

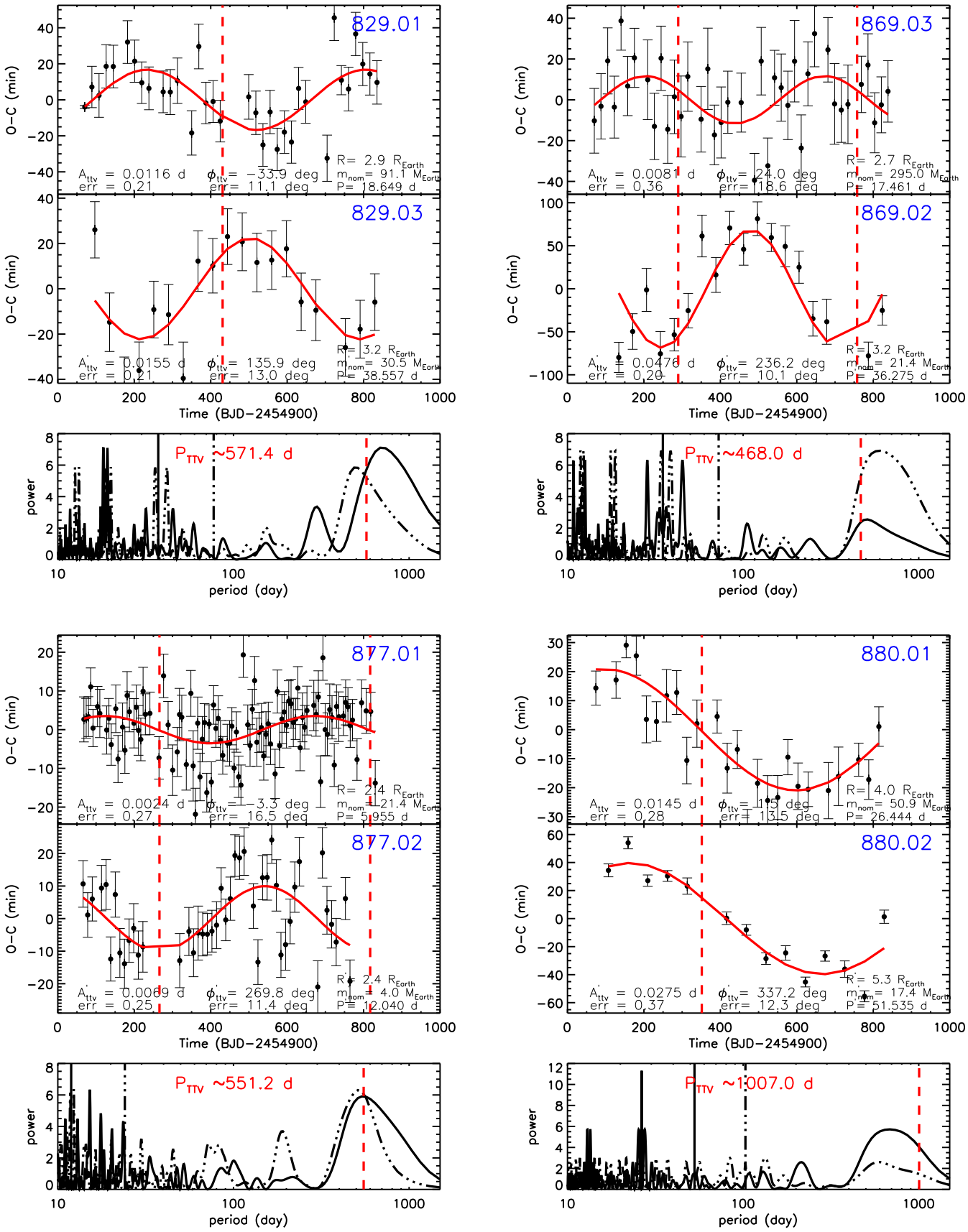

FIG. 3.— Similar to Fig.1, but for another four pairs.

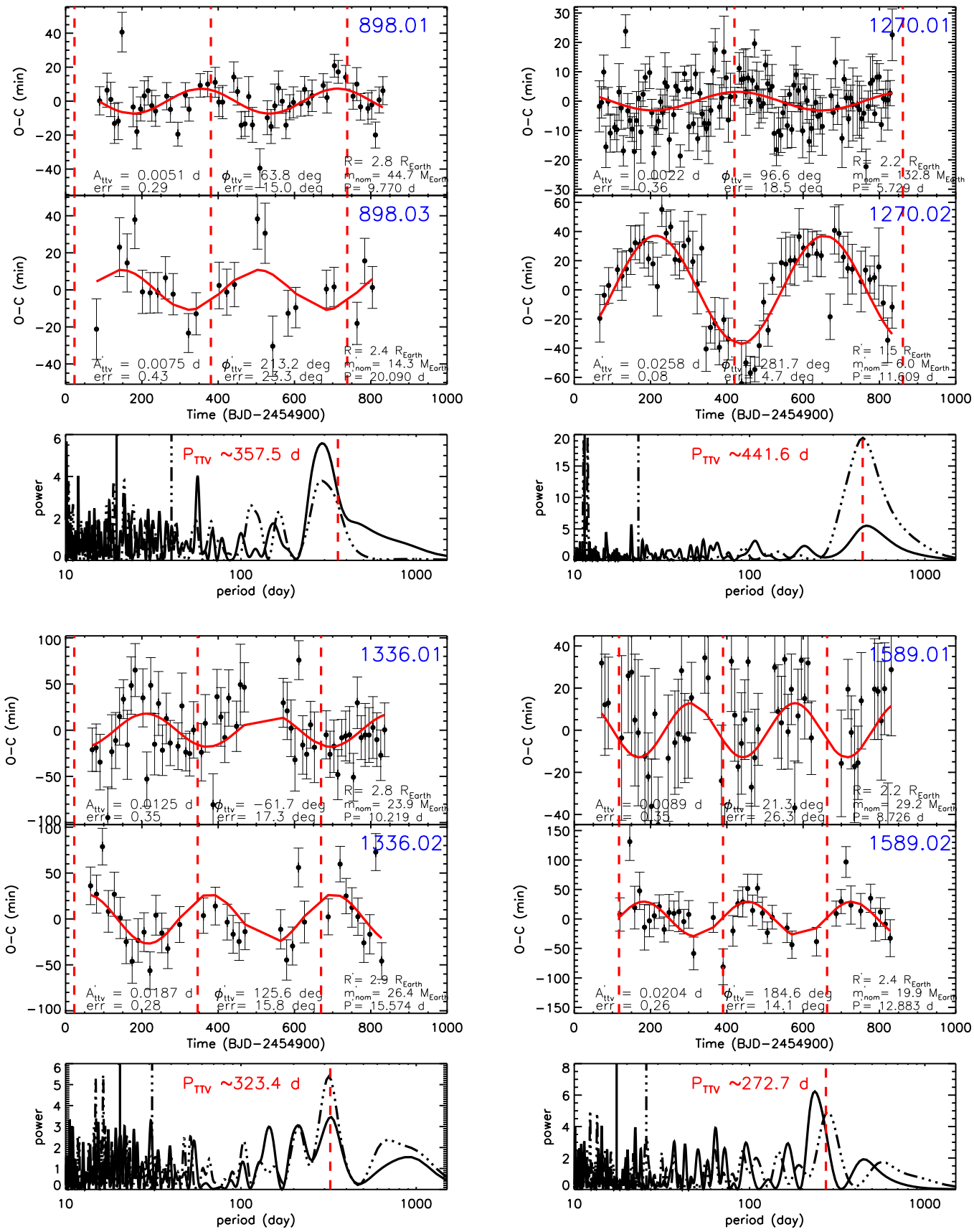

FIG. 4.— Similar to Fig.1, but for another four pairs.

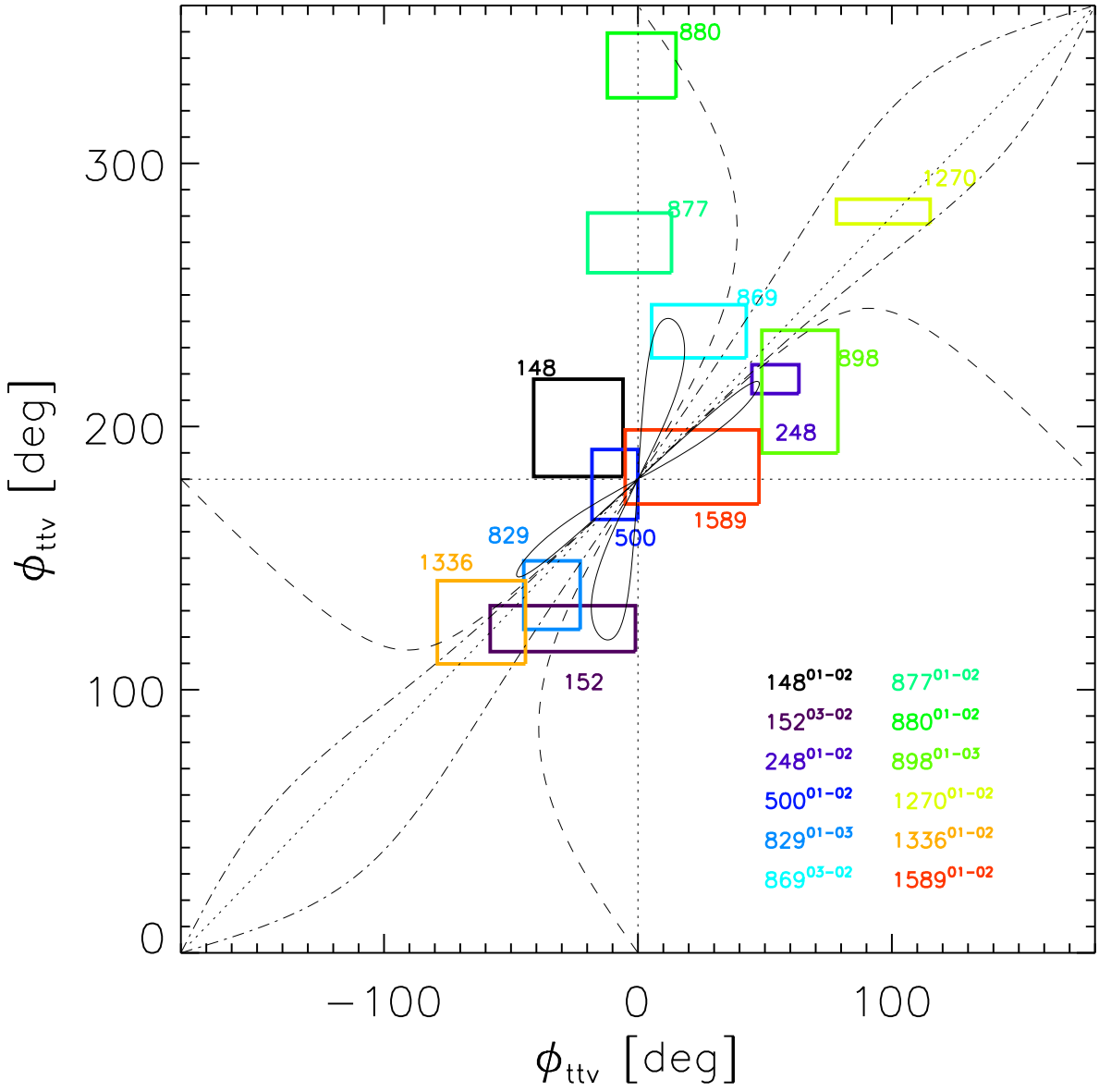

FIG. 5.— TTV phase diagram for 12 pairs of planets confirmed in this paper (see also in table 2). The x-value is the phase of the inner planet TTV, and y-value that for the outer planet. The width and height of each rectangle represent the 1-sigma uncertainty. A system with zero free eccentricity would lie at the center ($\phi V = 0, \phi V^{'} = 180°$). Systems of 2 : 1 resonance would lie at the top-left of Quadrant I or bottom-right of Quadrant III, whiles those of other first order resonances would lie at the bottom-right of Quadrant I and top-left of Quadrant III (separated by the inclined dot line). Quadrant II and IV are forbidden in theory. There are three curves in the 3:2 region, representing the theoretical prediction for the TTV phases when $|Z_{\rm free}| = \Delta$ (solid curve), $|Z_{\rm free}| = 1.5\Delta$ (dashed curve) and $|Z_{\rm free}| = 2\Delta$ (dot-dashed curve). Another three in the 2:1 region, corresponding to $|Z_{\rm free}| = 0.25\Delta$, 0.5Δ and Δ, respectively.

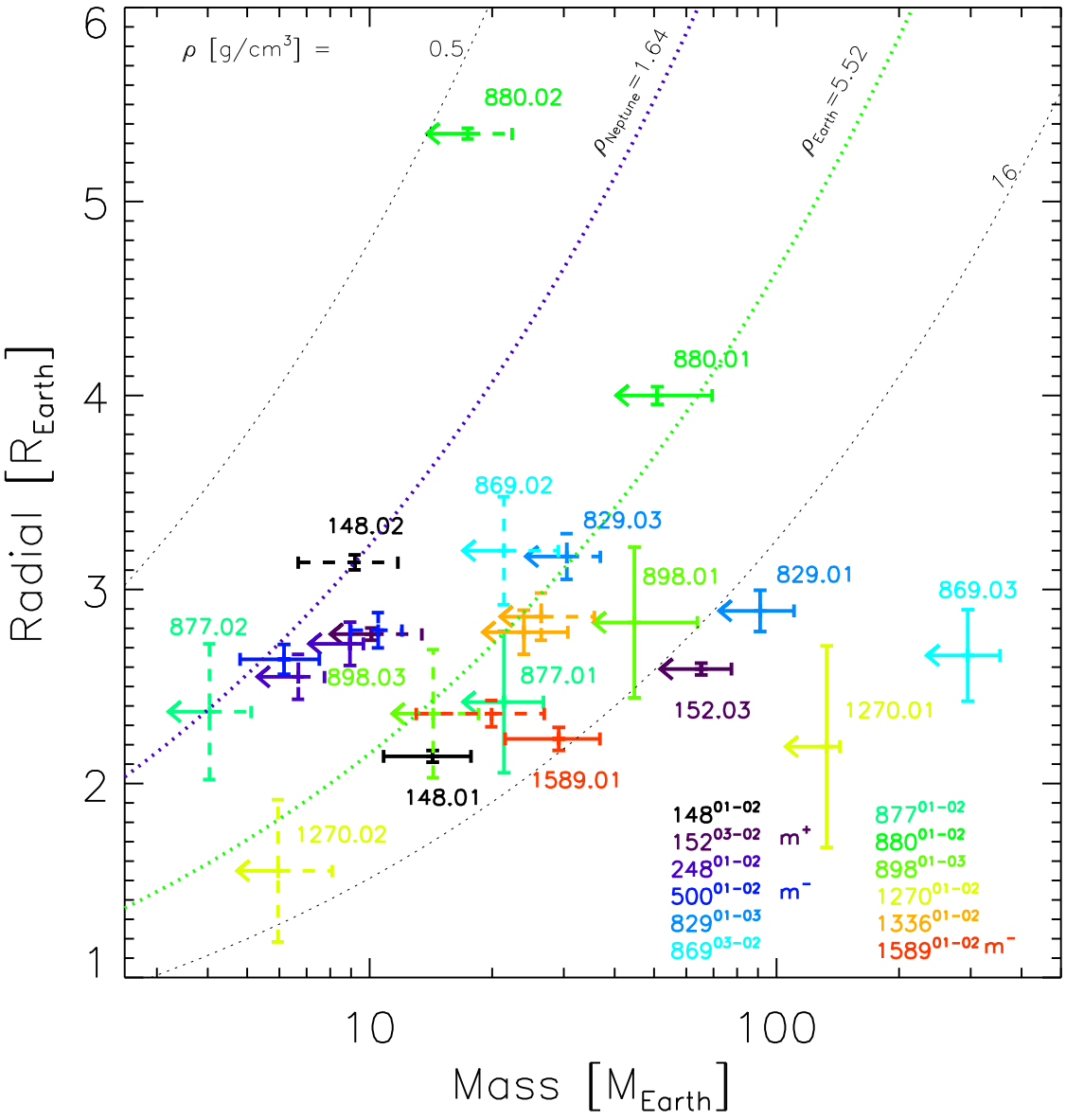

FIG. 6.— Mass-radius diagram for the 12 pairs confirmed in this paper. Different systems are plotted with different colours, and for each pair, the inner one is plotted with solid line style and the outer one with dashed style. The masses are the nominal mass computed using Eqn.8, their errors are estimated with the uncertainty of TTV amplitudes. The nominal masses are likely the true masses for KOI 148, 500 and 1589 but upper limits for the others (as shown by the left pointing arrows). The error estimates on radii (see also in table 1) shown here only reflect the uncertainties on the fitted planet-star radius ratio given by Batalha et al. (2012). We caution that the true uncertainties on planetary radii should be significantly larger (see §4.1). The superscripts, "m^+, m^-", have the same meaning as in table 1.

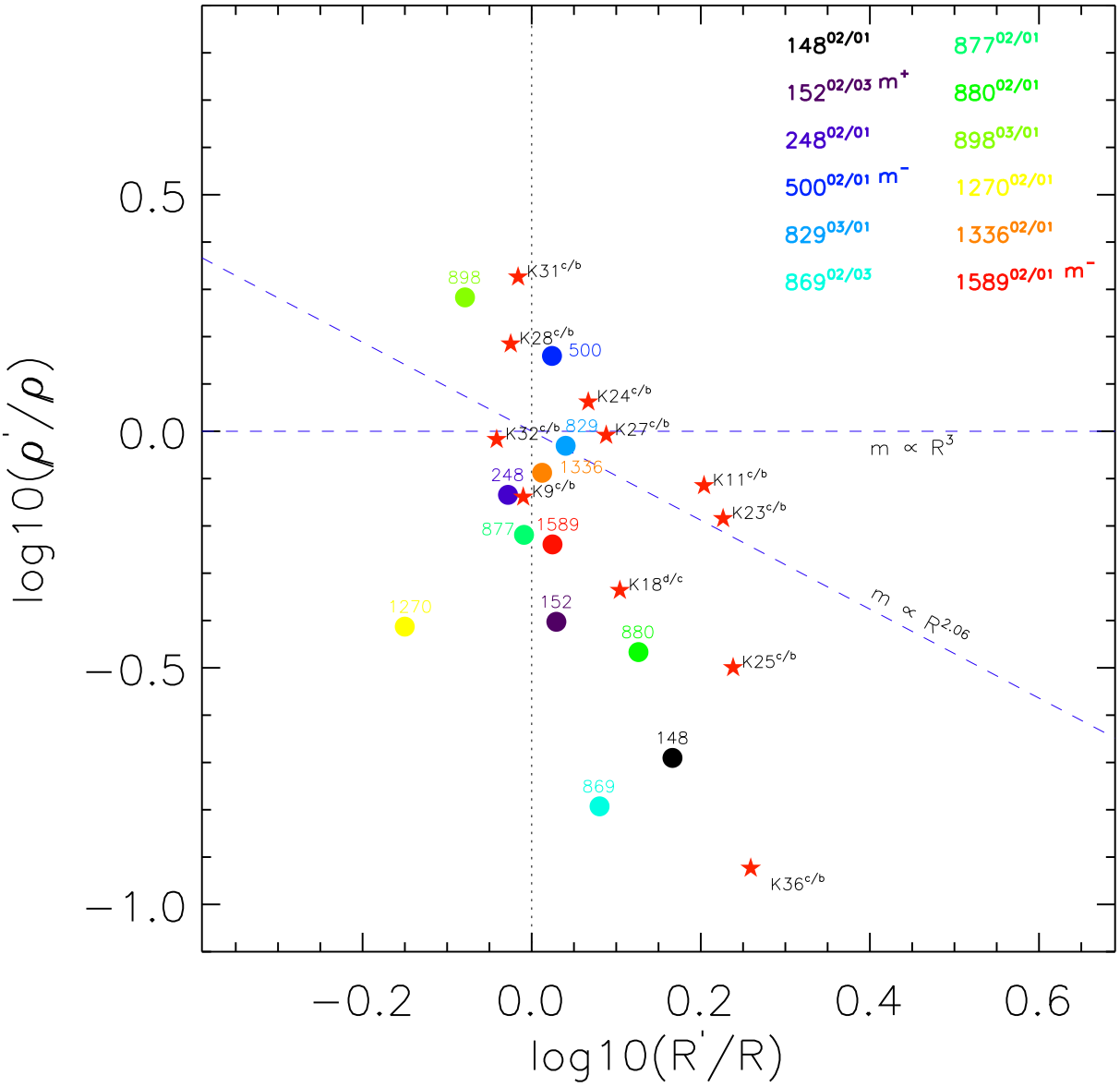

FIG. 7.— Density ratio (ρ'/ρ) vs. raids ratio (R'/R) for 12 pairs confirmed in this paper and 11 pairs of previous confirmed Kepler planets. Caution that the error bars (not plotted for clarity) of individual systems are large (see table 1), especially for KOI 869, 877, 898 and 1270. The masses used for the other 11 pairs are adopted from Holman et al. (2010); Lissauer et al. (2011b); Fabrycky et al. (2012a); Nesvorný et al. (2012), and many of them are also subject to large uncertainties. The superscripts, "m^+, m^-", have the same meaning as in table 1.

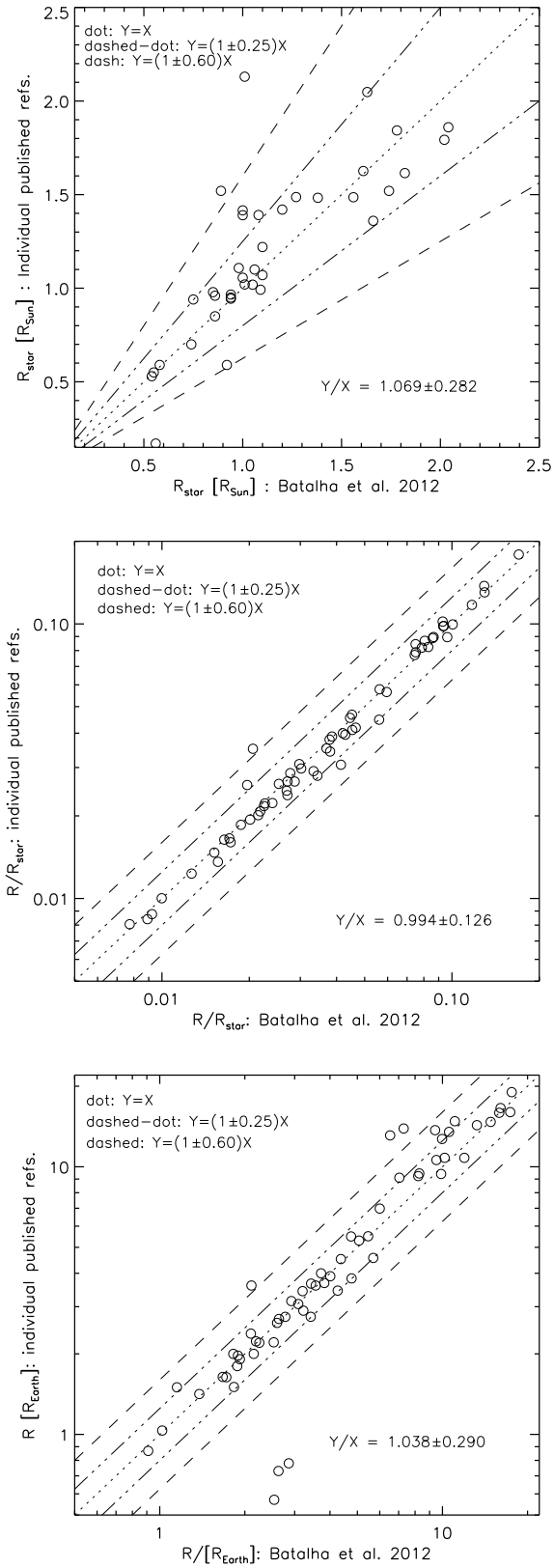

FIG. 8.— The stellar radii (top), planet-star radius ratios (middle) and planetary radii (bottom) from individual published references (Y axis, summarized at http://kepler.nasa.gov/Mission/discoveries/) vs. those (X axis) given by the KOI catalog (Batalha et al. 2012). In the top panel, we consider 37 stars from Kepler 4 to 46. Note, Kepler 10 counts twice because two references Batalha et al. (2011); Fressin et al. (2011) give two different radii. Kepler 16, 34 and 35 are binary stars and not plotted here. As of today, there is no system named after Kepler 13, 37, 38. In the middle and bottom panels, we consider 60 confirmed Kepler planets in total. At bottom-right of each panel, we print the average ± standard deviation of the ratio between values Y and X. Such analyses provide a simple diagnosis to the uncertainties of stellar radius, planet-star radius ratio and planetary radius.

TABLE 1
Key Properties of Planets and Stars of 12 Systems.

koi[a]	id	id′	P	P'	R^b	R'^b	$m_{\rm nom}{}^c$	$m'_{\rm nom}{}^c$	m'/m^d	ρ'/ρ^e	$M_\star{}^f$	$R_\star{}^g$
-	-	-	d	d	$R_\oplus$	$R_\oplus$	$M_\oplus$	$M_\oplus$	-	-	$M_\odot$	$R_\odot$
148	1	2	4.778	9.674	2.1(1±0.01)	3.1(1±0.01)	14.3(1±0.24)	9.2(1±0.27)	0.64(1±0.52)	0.20(1±0.60)	0.89	0.89
152^{m+}	3	2	13.485	27.403	2.6(1±0.01)	2.8(1±0.01)	65.3(1±0.19)	10.1(1±0.33)	0.48(1±0.52)	0.40(1±0.59)	1.07	0.99
248	1	2	7.204	10.913	2.7(1±0.04)	2.5(1±0.05)	8.9(1±0.08)	6.7(1±0.16)	0.60(1±0.24)	0.73(1±0.50)	0.55	0.53
500^{m-}	1	2	7.053	9.522	2.6(1±0.03)	2.8(1±0.03)	6.2(1±0.22)	10.5(1±0.14)	1.70(1±0.36)	1.44(1±0.55)	0.72	0.65
829	1	3	18.649	38.557	2.9(1±0.04)	3.2(1±0.04)	91.1(1±0.21)	30.5(1±0.21)	1.23(1±0.42)	0.93(1±0.64)	0.97	0.89
869	3	2	17.461	36.275	2.7(1±0.09)	3.2(1±0.09)	295.0(1±0.20)	21.4(1±0.36)	0.28(1±0.56)	0.16(1±1.09)	0.79	0.82
877	1	2	5.955	12.040	2.4(1±0.15)	2.4(1±0.15)	21.4(1±0.25)	4.0(1±0.27)	0.57(1±0.52)	0.60(1±1.41)	0.63	0.59
880	1	2	26.444	51.535	4.0(1±0.01)	5.3(1±0.01)	50.9(1±0.36)	17.4(1±0.28)	0.82(1±0.65)	0.34(1±0.70)	0.93	0.91
898	1	3	9.770	20.090	2.8(1±0.14)	2.4(1±0.14)	44.7(1±0.43)	14.3(1±0.29)	1.11(1±0.72)	1.92(1±1.55)	0.66	0.61
1270	1	2	5.729	11.609	2.2(1±0.24)	1.6(1±0.24)	132.8(1±0.08)	6.0(1±0.36)	0.14(1±0.44)	0.39(1±1.86)	0.83	0.73
1336	1	2	10.219	15.574	2.8(1±0.04)	2.9(1±0.04)	23.9(1±0.28)	26.4(1±0.35)	0.89(1±0.63)	0.82(1±0.88)	0.95	1.03
1589^{m-}	1	2	8.726	12.883	2.2(1±0.03)	2.4(1±0.03)	29.2(1±0.26)	19.9(1±0.35)	0.68(1±0.61)	0.58(1±0.77)	0.96	0.99

[a] Superscirpt "m+" denotes that TTV analysis of KOI 152.03-02 is likely contaminated by the resonance chain induced by KOI 152.01 and the masses shown here might not fully reflect their true masses and "m-" denotes that the resonance chain effect is less important to the TTV analyses of KOI 500.01-02 and KOI 1589.01-02.
[b] Adopted from Batalha et al. (2012), and the uncertainties are only the error bars of planet-star radius ratio.
[c] Deduced from Eqn.8, which are likely the true mass for system KOI 148, 500 and 1589 but upper limits for others.
[d] Deduced from Eqn.9 and each error bar is computed as the sum of TTV amplitude errors of the pair. Note this ratio could differ a lot compared to the ratio of nominal masses, especially for the case of 2:1 MMR.
[e] Deduced from the above mass ratios and radii. Note density ratio is independent on the uncertainty of stellar radius.
[f] Deduced from the stellar radii and surface gravity reported from Batalha et al. (2012).
[g] Adopted from Batalha et al. (2012).

TABLE 2
Results of TTV Analyses for 12 Pairs of Planets

KOI[a]	id	id′	j	P	P'	Δ	P^j	$A_{\rm ttv}$	$A'_{\rm ttv}$	$\phi_{\rm ttv}$	$\phi'_{\rm ttv}$	$\chi_{\rm red}$	$\chi'_{\rm red}$
-	-	-	-	d	d	-	d	d	d	deg	deg	-	-
148	1	2	2	4.778	9.674	0.012	392.0	0.0028(1±0.27)	0.0023(1±0.24)	-23.5±17.6	199.5±18.5	1.4	1.2
152^{m+}	3	2	2	13.485	27.403	0.016	851.9	0.0055(1±0.33)	0.0182(1±0.19)	-29.6±28.6	123.2± 8.7	1.2	1.1
248	1	2	3	7.204	10.913	0.010	367.7	0.0064(1±0.16)	0.0139(1±0.08)	54.1± 9.3	218.0± 5.5	1.3	0.9
500^{m-}	1	2	4	7.053	9.522	0.012	191.1	0.0059(1±0.14)	0.0049(1±0.22)	-9.1± 9.0	178.0±13.3	1.3	1.7
829	1	3	2	18.649	38.557	0.034	571.4	0.0116(1±0.21)	0.0155(1±0.21)	-33.9±11.1	135.9±13.0	1.2	1.1
869	3	2	2	17.461	36.275	0.039	468.0	0.0081(1±0.36)	0.0476(1±0.20)	24.0±18.6	236.2±10.1	1.0	1.9
877	1	2	2	5.955	12.040	0.011	551.2	0.0024(1±0.27)	0.0069(1±0.25)	-3.3±16.5	269.8±11.4	1.2	1.4
880	1	2	2	26.444	51.535	-0.026	1007.0	0.0145(1±0.28)	0.0275(1±0.36)	1.5±13.5	337.2±12.3	1.3	3.2
898	1	3	2	9.770	20.090	0.028	357.5	0.0051(1±0.29)	0.0075(1±0.43)	63.8±15.0	213.2±23.3	1.2	1.2
1270	1	2	2	5.729	11.609	0.013	441.6	0.0022(1±0.36)	0.0258(1±0.08)	96.6±18.5	281.7± 4.7	1.4	1.1
1336	1	2	3	10.219	15.574	0.016	323.4	0.0125(1±0.35)	0.0187(1±0.28)	-61.7±17.3	125.6±15.8	1.1	1.4
1589^{m-}	1	2	3	8.726	12.883	-0.016	272.7	0.0089(1±0.35)	0.0204(1±0.26)	21.3±26.3	184.6±14.1	1.2	1.2

[a] superscripts "m+" and "m-" have the same meaning as in table 1.

APPENDIX

TTV DATA

The TTV data are available at www...